A framework to improve the alignment of individual cytoarchitectonic maps of the Julich-Brain atlas using cortical folding landmarks

Xiaoyu Wang, Yann Leprince, Jessica Lebenberg, Clement Langlet, Hartmut Mohlberg, Denis Rivière, Guillaume Auzias, Timo Dickscheid, Katrin Amunts, Jean-François Mangin

Cerebral Cortex, 2023, pp. 1–14

doi: DOI HERE
Advance Access Publication Date: Day Month Year
Paper

PAPER

A framework to improve the alignment of individual cytoarchitectonic maps of the Julich-Brain atlas using cortical folding landmarks

Xiaoyu Wang,[1] Yann Leprince,[1,2] Jessica Lebenberg,[1,3] Clement Langlet,[1] Hartmut Mohlberg,[4] Denis Rivière,[1] Guillaume Auzias,[5] Timo Dickscheid,[4,6] Katrin Amunts[4,7] and Jean-François Mangin[1,*]

[1]Université Paris-Saclay, CEA, CNRS, Neurospin, Baobab, Saclay, France, [2]UNIACT, NeuroSpin, CEA, Université Paris-Saclay, F-91191, Gif-sur-Yvette, France, [3]Lariboisière University Hospital, APHP, Translational Neurovascular Centre and Department of Neurology, FHU NeuroVasc, Paris, France, [4]Institute of Neuroscience and Medicine (INM-1), Research Centre Jülich, 52425, Jülich, Germany, [5]Institut de Neurosciences de la Timone, UMR 7289, Aix Marseille Université, CNRS, Marseille, France, [6]Institute of Computer Science, Heinrich-Heine University Düsseldorf, 40225, Düsseldorf, Germany and [7]Cecile und Oskar Vogt Institut für Hirnforschung, University Hospital Düsseldorf, Heinrich-Heine Universität Düsseldorf, 40225, Düsseldorf, Germany
[*]Corresponding author. jfmangin@gmail.com
FOR PUBLISHER ONLY Received on Date Month Year; revised on Date Month Year; accepted on Date Month Year

Abstract

The segregation of the cortical mantle into cytoarchitectonic areas provides a structural basis for the specialization of different brain regions. In vivo neuroimaging experiments can be linked to this postmortem cytoarchitectonic parcellation via Julich-Brain. This atlas embeds probabilistic maps that account for inter-individual variability in the localization of cytoarchitectonic areas in the reference spaces targeted by spatial normalization. We built a framework to improve the alignment of architectural areas across brains using cortical folding landmarks. This framework, initially designed for in vivo imaging, was adapted to postmortem histological data. We applied this to the first 14 brains used to establish the Julich-Brain atlas to infer a refined atlas with more focal probabilistic maps. The improvement achieved is significant in the primary regions and some of the associative areas. This framework also provides a tool for exploring the relationship between cortical folding patterns and cytoarchitectonic areas in different cortical regions to establish new landmarks in the remainder of the cortex.

Key words: Cytoarchitectonic parcellation, cortical folding landmarks, postmortem brains, sulcal-based alignment, Julich-Brain atlas

INTRODUCTION

Cytoarchitecture, which refers to the spatial distribution and morphology of cell bodies and their arrangement into structures such as cortical layers, is a fundamental principle of brain organization. The cortex can be subdivided into areas based on its cytoarchitectonic features. Cytoarchitecture correlates with other aspects of brain organisation such as connectivity, molecular architecture or gene express, which suggests that they have specific roles in the functional organisation of the brain (Amunts and Zilles, 2015). Therefore, researchers are seeking to link the cytoarchitecture to functional activation maps (Passingham et al., 2002; Eickhoff et al., 2006) and/or brain connectivity (Wei et al., 2018). Unfortunately, details of the cytoarchitecture are not accessible with in vivo imaging, owing to limitations in spatial resolution, but only via postmortem microscopy. Therefore, it is not possible to compare the cytoarchitectonic and functional maps directly for the same living individual. This is why exploring the links between functional and cytoarchitectonic areas requires a statistical approach based on spatial normalization, which involves aligning brains before comparing them (Eickhoff et al., 2006). This indicates that brains imaged using different techniques (in vivo MR, postmortem MR, and histology) and from different subjects need to be aligned. Several brains that differ in shape, sulcal pattern, and microstructure should be aligned to obtain a representation of inter-individual variability in brain structure. This alignment results in the representation of the areas in a common reference coordinate system. For either in vivo MRI activations or postmortem cytoarchitectonic data, probabilistic maps of the areas can be constructed by aligning the set of brains with a template brain. For cytoarchitectonic probabilistic maps, the community has access to an outstanding atlas, the Julich-Brain, resulting from decades of microscopic work requiring a high level of expertise

performed on sections of 23 postmortem brains (Amunts et al., 2020). This atlas resulted from the 3D alignment of 23 postmortem brains with templates representing the MNI Colin27 or MNI ICBM 152 2009c Nonlinear Asymmetric (ICBM152casym) reference spaces, using a volume-based elastic 3D alignment method (Hömke, 2006).

Although this strategy has been very efficient, the current Julich-Brain atlas cannot resolve all the ambiguities concerning the pairings between architectonic areas and functional activations, particularly for small or thin elongated areas. The shapes of these areas are close to the spatial resolution of the template (1 mm). Considerable inter-individual variability in the topography and size of architectonic areas creates a significant overlap between their probabilistic representations. With regard to the cortex, this difficulty is amplified by several uncertainties about the links between the location of the architectonic areas and the morphology of cortical folding, the main information implicitly driving the alignment of the brains making up the Julich-Brain atlas. Moreover, the considerable inter-individual variability in cortical folding disturbs the results of standard alignment tools (Mangin et al., 2016). The alignment of histological 3D reconstructions, which have different contrasts, distributions of gray values, geometrical deformation due to acquisition, etc. is even more challenging (Alkemade et al., 2020). Consequently, the major sulci that are landmarks of interest for predicting the location of architectural areas were not always correctly aligned across the 23 brains, although the major sulci of primary areas represent consensual landmarks for architectonics. The link between cortical folding and inter-subject variability has been demonstrated using an alternative two-dimensional probabilistic approach involving the alignment of cortical surfaces rather than 3D brains (Fischl et al., 2008). Nevertheless, the question is complex, insofar as comparable studies are missing in most higher associative areas. Some authors have assumed that there is no link between architectonics and folding in associative areas (Zachlod et al., 2023). An alternative hypothesis is that the significant variability in folding in these regions is related to the existence of different topographies of the architectonic areas.

To address this hypothesis, this paper applies a framework described in (Lebenberg et al., 2018) that aims to improve the accuracy of alignment between postmortem architectonic maps and in vivo functional data using information from cortical folding. The idea was to replace standard alignment procedures that use information from the entire cortical folding pattern, regardless of the predictive value of each sulcus for architectonics, with the individual alignment of specific sulci. In addition, the precise alignment of these sulci must be guaranteed during the creation of the architectonic probabilistic atlas and during its projection onto in vivo brains. No solution exists when a standard alignment method fails to align an important sulcus with its fellow sulci across the brains. The proposed framework allows the user to act on the alignment behavior and control the result in terms of sulcus alignment.

The framework described in this paper is based on two pre-existing tools from the BrainVISA package: Morphologist, a pipeline for automatically defining 125 sulci from T1-weighted MRI (Perrot et al., 2011), and DISCO, a second pipeline for aligning a set of predefined sulci across a group of brains (Auzias et al., 2011), which has not been part of the publicly distributed package for several reasons, including the complexity of use, but mainly licensing issues for the MATLAB code. This second pipeline initializes the cross-brain alignment performed by a well-established method used in this study, DARTEL, a pipeline from the SPM package. This set of tools has been previously used in the context of the Human Brain Project (HBP) (Lebenberg et al., 2018) to align various templates that are too different to achieve precise sulcus alignment using conventional methods (Colin27 individual template, ICBM152casym group template, postmortem BigBrain (Amunts et al., 2013) and infant template (Kabdebon et al., 2014)). The same framework was used to create and align templates of several great ape species with the ICBM152casym human template, using sulci common to all species (Leprince et al., 2020).

In this study, we built upon the same framework to align a set of 14 Jülich postmortem human brains toward the ICBM152casym template. The main challenge was to apply the Morphologist pipeline to 3D reconstructions of gray and white classifications of histological images provided by the Jülich team's standard workflow. These classifications did not always match the quality of the BigBrain classifications, probably because of the wider gaps between sections. This study required numerous manual adjustments, particularly to deal with the topological 3D inconsistencies relative to the folding morphology. Subsequently, a set of sulci that was sufficiently stable to be reliably identified in all 14 postmortem brains and in the template brain ICBM152casym was selected for use as alignment constraints by the DISCO pipeline. This set, chosen from the 125 sulci automatically defined by the Morphologist pipeline (Figure 11), corresponds to the subset previously used in the context of alignment of the HBP reference spaces (Lebenberg et al., 2018). This corresponds either to sulci from primary areas, which are reasonably stable across subjects, or to the major furrows of associative areas. Smaller sulci in the associative areas are highly variable and difficult to define unambiguously in postmortem or average template brains.

After the estimation of the DISCO+DARTEL sulcus-based transformations toward the ICBM152casym space, all the areal cytoarchitectonic maps from the 14 brains were transformed into this reference space to build a new release of the architectonics probabilistic areas, and finally the maximum probability atlas (Amunts et al., 2020). The results show that our proposed method can effectively align postmortem brains and minimize the dispersion of targeted sulci; therefore, some cytoarchitectonic areas of the maximum probability atlas related to the selected sulci have better spatial topography than those of the conventional Julich-Brain.

Our framework also provides an original 3D visualization tool (see online 3D visualization tool) (Cointepas et al., 2001) for browsing 14 brains simultaneously with 3D views, including individual architectonic maps and representations of the sulci (Rivière et al., 2022). This tool will make it possible to carry out a systematic study of the links between sulci and architecture. This will enable us to draw up an optimal list of sulci to be included in the DISCO alignment in the future. It could also lead to question the identification of certain sulci in individuals whose architectonic organization seems incompatible with most individuals. The inter-individual variability in folding patterns could lead to inconsistencies in sulcus identification. In situations in which sulcus identification cannot be challenged, an alternative strategy would be used to define the regional variants of the cytoarchitectonic probabilistic atlas for subgroups of individuals with specific folding patterns.

MATERIALS AND METHODS

Database

This study was performed on the 14 first postmortem human brains used in Jülich (Amunts et al., 2020), as shown in Supplementary Table 1. For each brain, we used a grey/white map computed from a 3D reconstructed histological dataset aligned to the single subject MNI-Colin27 template using linear transformation. This 3D histological reconstruction stemmed from a complex iterative procedure involving a low quality postmortem MRI and often also a blockface 3D volume. These two complementary datasets help to achieve a consistent 3D alignment of the 2D histological sections performed at a spatial resolution of 0.3 mm corresponding to the distance between analyzed sections (only one every 15th is analyzed). Once the 3D consistency was achieved for the 3D histological volume, it was converted into grey/white map and aligned with the Colin27 template. For the framework described in this paper, this alignment is only linear, but to deliver the Julich-Brain atlas, a nonlinear alignment was performed. The goal of this paper is to propose an alternative nonlinear alignment informed by annotations of sulcus-based landmarks. The grey/white maps account for the partial volume effect resulting from the transformation of high resolution histological images toward a lower resolution.

These 14 brains cover most of the cytoarchitectonic areas that have been mapped in the past, whereas a smaller number of areas have been mapped in other postmortem brains, from a total of 23 brains (Amunts et al., 2020). The probabilistic maps of the Julich-Brain atlas were each generated from 10 brains selected out of 23, including 5 males and 5 females, chosen based on their compatibility in terms of topography, tissue quality, and other factors. Considering that processing histological data is highly time- and labor-intensive, we chose to present the first validation of our research program using only these 14 brains.

Data pre-processing

Owing to histological processing, staining artifacts, small ruptures, or section folding are unavoidable. To overcome artifacts in the histology-based gray/white matter maps, before performing sulci extraction and sulcal-based alignment, a dedicated semi-automatic cleaning procedure based on mathematical morphology and manual drawing was performed for each brain. For example, we separated the cerebral ventricles from the background and deleted voxels labelled as white matter located within 2 mm of the background, which was anatomically impossible. In addition, we used a map of the geodesic distance from the background to any white matter voxel to detect and delete spurious connections from the white matter to outside the brain. All these procedures were performed using the Aims and Vip commands of the BrainVISA package. For some brains with lower quality gray/white maps, several such connections were detected and had to be corrected via manual drawing using the Anatomist visualization software to fix the 3D topography of the gray and white matter. We show in Figure 1a, b a 2D slice of 3D gray and white matter maps of a brain before and after the cleaning procedure.

Extraction of sulci

Sulci have to be extracted from the gray/white matter maps for each subject and the ICBM152casym template to perform sulcal-based alignment. To obtain this information, brain images were processed using the freely available "Morphologist 2021" pipeline (Fischer et al., 2012) of BrainVISA software (http://brainvisa.info/web/index.html, (Cointepas et al., 2001)). This pipeline can segment the gray and white matter respectively through histogram analyses and morphological operations applied to a bias-corrected T1-weighted MR image. It also computes a skeleton-based negative cast of the cortex, providing a representation of the elementary folds. In this study, the inputs of the Morphologist pipeline for the postmortem brains are 3D corrected gray/white matter maps, not T1-weighted MR images. The main steps of the pipeline are illustrated in Figure 2. After the split of the skeleton into a set of elementary folds using topological properties, the 125 sulci shown in Supplementary Figure 11 were automatically labelled using a template-based Bayesian pattern recognition system (Perrot et al., 2011). This machine learning system did annotate from BrainVISA's nomenclature each elementary fold. Finally, we performed a careful inspection of the automatic labelling in order to perform manual corrections, to get rid of potential errors of the sulcus recognition process of BrainVISA. It should be noted that BrainVISA's machine learning system for sulcus annotation has been trained from in vivo MRI and could be disturbed when fed with the postmortem histological datasets. We do not claim that our final labeling is indisputable in the most variable regions. One of our future goals is to use this framework to improve the identification of sulci in unusual configurations using architectural area localization.

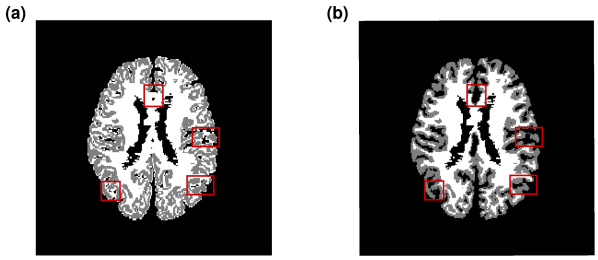

Fig. 1. 2D slice of 3D gray/white matter maps of brain 11 before and after the dedicated cleaning procedure. (a) Original gray/white maps inferred from histological sections; (b) Corrected gray/white maps. The red boxes show some examples of corrections.

The ICBM152casym template was processed with the standard Morphologist pipeline to obtain the sulcus-based target to align the postmortem brains with this reference space.

Registration pipeline

DISCO

The DISCO algorithm, described in detail in (Auzias et al., 2011), consists of three main steps: 1) The sulcal imprints (the top and bottom lines of each sulcus used as alignment constraints) are extracted for each subject. 2) All the imprints are aggregated into an initial empirical template using the affine alignment of subjects. 3) Each individual sulcal imprint is registered from its native space onto the empirical template using smooth invertible deformations (Glaunes et al., 2004). 4) The deformed imprints are aggregated into an updated empirical template for iterating Steps 3) and 4) until convergence, that is, when the distance between two consecutive templates is lower than a predetermined threshold.

In this study, we used DISCO embedded in a toolbox of BrainVISA 5.0.4 (still at the beta level). The deformation fields

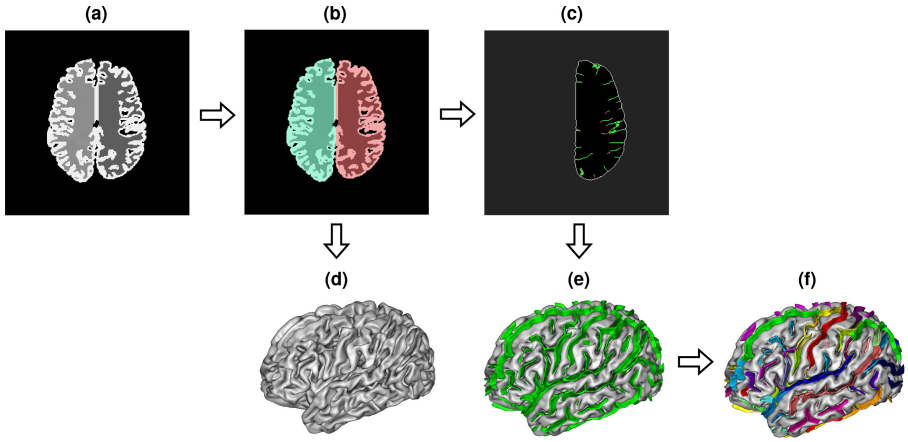

Fig. 2. Overview of the main steps of the BrainVISA/Morphologist pipeline. (a) Corrected gray/white matter maps; (b) Segmentation of the two hemispheres; (c) Skeleton representation of the folding graph of the left hemisphere; (d) Mesh representation of the white matter of the left hemisphere; (e) Folding graph that represents the elementary folds, which is the negative cast of (d) and (f) sulci labeled by a template-based Bayesian pattern recognition system.

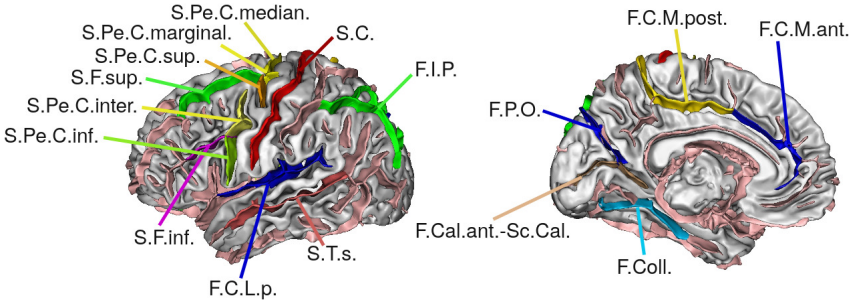

Fig. 3. Sulci on the ICBM152casym template to drive the DISCO alignment for the 14 Jülich postmortem brains.

were computed using the functions in MATLAB R2014a. The value of the DISCO regularization parameter "coef_sigV" was adjusted from 20 to 30 millimetres to impose more regularity on the results, and the other parameters were set to default.

Sulci chosen to drive the DISCO alignment were selected throughout the whole brain to achieve a reasonable spatial coverage of constraints. We chose 16 stable sulci that are located around the primary areas, as shown in Figure 3, and some major furrows in the associative areas. These sulci are the less variable across individuals and thus easier to identify. It should be noted that all of the precentral sulcus (S.Pe.C.median., S.Pe.C.marginal., S.Pe.C.sup., S.Pe.C.inter., S.Pe.C.inf.) are regrouped under one label (S.Pe.C.) and actually considered as one constraint by DISCO, the same is the case with all of the calloso-marginal fissure (F.C.M.).

DARTEL

The DARTEL algorithm, which is a volumetric spatial registration method, is fully introduced in (Ashburner, 2007). It is widely used in the neuroscience community, and provides better alignment than most alternatives in several cases (Klein et al., 2009; Yassa and Stark, 2009). DARTEL embeds an iterative alignment process akin to DISCO's strategy, repeating the template building and alignment of each individual brain onto the template. Similar to DISCO, DARTEL uses diffeomorphisms to align the subjects with the evolving template. The alignments of the gray and white matter maps are simultaneously optimized. The quality of the initial rough alignment of individual brains, which is usually based on affine alignment, is important for avoiding local minima issues. In the context of this study, we initialized DARTEL with the alignment achieved by DISCO, in order to force the local minimum to align the preselected sulci. It should be noted that DARTEL is not the only possible tool for our framework, which essentially aims to provide initialization based on folding landmarks for a high-performance inter-subject registration tool. The use of other tools may have led to similar results.

In our study, the DARTEL algorithm was applied using the standalone version of SPM12 software (Statistical Parametric Mapping). The linear elastic regularization parameters of all iterations were set to four times the default values to ensure that the deformations were sufficiently smooth. Gray and white matter binary data, which were aligned using the DISCO process, were used as inputs for this algorithm. All the inputs were resampled into an identical matrix ($200 \times 245 \times 180$) with an isotropic spatial resolution (1 mm) to satisfy the requirements of DARTEL.

Maximum probability atlas generation

In this study, we chose to align the individual architectural maps directly with the average ICBM template, rather than with the Colin27 individual template, as historically done by

the Jülich team (Amunts et al., 2020). The aim is to avoid biases induced by idiosyncrasies of this individual brain. The major sulci of the average ICBM template have simplified shapes, with few interruptions. To build the 3D maximum probability atlas of the cytoarchitecture in the ICBM152casym reference space, we first transformed the individual areal maps and Gap Maps toward the ICBM152casym template using the previously computed DISCO+DARTEL transformations. The Gap Maps correspond to the connected components of the part of the cortex that have not yet been architectonically mapped (Amunts et al., 2020). We then replicated the strategy used to build the Julich-Brain atlas. The fraction values corresponding to the partial volume effect were normalized for each area (values ranging from 0 to 255 normalized from 0.0 to 1.0) in the reference space and a threshold of 0.1 (the same one used by Jülich (Amunts et al., 2020)) was applied to create the binary individual maps. The binary individual maps were then superimposed on the reference space, and probabilistic cytoarchitectonic maps were generated and stored as volume data files with values ranging from 0.0 to 1.0. These values encode the probability of an area (0% to 100% overlap between subjects) being localized at a specific spatial position. After that, a spatial Gaussian smoothing with a full width at half maximum of 3 mm was applied to these probabilistic cytoarchitectonic maps. Subsequently, a threshold of 0.4 (same as that for the Julich-Brain atlas) was applied to only retain voxels that contained more than 40% of the brains. The maximum probability maps (MPMs) of the left and right hemispheres were calculated by assigning each voxel of the ICBM152casym template brain to the area with the highest probability in that voxel (Eickhoff et al., 2005, 2006). If two areas shared the same probability in a particular voxel, the voxel was assigned to the area with the higher average probabilities in directly adjacent voxels (Eickhoff et al., 2005, 2006). These MPMs present a contiguous, non-overlapping parcellation of the entire cortex and reflect the most likely area at that position for each voxel.

Evaluation of alignment

To compare the alignment procedures quantitatively, as in the seminal work of the HBP (Lebenberg et al., 2018), we used two indices that were computed after each alignment step and for all the experiments in this study.

Pairwise Dice criteria

We used the pairwise Dice criteria (Dice, 1945) to measure the overlap of the cortical mantle. The closer the score is to 1, the better the deformation is adapted to compensate for morphological differences between the brains.

Mean pairwise distances

We used the mean pairwise distances between the sulci computed from the sulcal imprints across all 14 individual brains to evaluate the dispersion for each sulcus chosen to drive the DISCO alignment. Mean distances were measured using the original voxels representing both the bottom line and hull junction of each sulcus. For each voxel of one brain, the closest voxel belonging to another brain was estimated, and the mean distance was then calculated from all voxel-based distances. The smaller the distance, the better was the alignment of the sulci across brains. It is worth noting that mean distances are more effective than Hausdorff distances in discarding the effects of idiosyncratic branches that cannot be aligned across brains.

RESULTS

Using eight cores of Intel Xeon E5-2620 v4 2.1 GHz processor, sulcal imprint extraction and optimized template building using the DISCO algorithm were completed in approximately 52 min for the 14 brains. Regardless of the initialization, the DARTEL algorithm was completed for the 14 brains in approximately 5 h 20 min.

Cerebral cortex overlapping

As expected, the inter-individual differences in the detailed morphology of the cortical mantle were not compensated after the affine or DISCO deformations (cf. Figure 4). DARTEL high-resolution alignment is required for this purpose. Notably, Figure 4a shows that initializing DARTEL with DISCO outputs increased the median Dice score to 0.648 with DISCO initialization versus 0.625 with affine initialization. This result shows that the initialization of DARTEL from the outcome of DISCO enables to reach a better optimal alignment, therefore avoiding suboptimal local minima that can be visited by the optimization of DARTEL when initialized using the usual affine initialization.

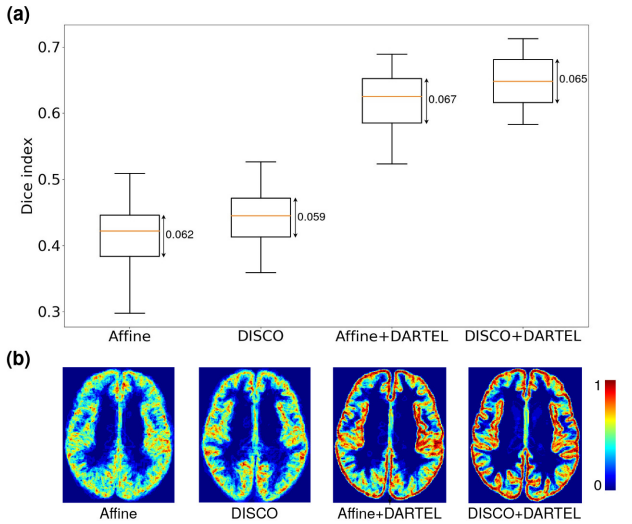

Fig. 4. Cerebral cortex overlapping across the 14 brains. **(a)** Distribution of the pairwise Dice scores computed after an affine deformation to the ICBM reference space, the DISCO alignment, the DARTEL alignment initialized with an affine transformation, and the DARTEL alignment initialized with the DISCO deformation; **(b)** normalized average map of the cortical layer over the whole 14 brains after each alignment.

Sulcal dispersion

Figure 5 shows the superimposition of all the sulci constraining the DISCO alignment before DISCO, after DISCO, and after DISCO+DARTEL deformation on the ICBM template. This visualization shows that DISCO aligned the preselected sulci sufficiently to provide a good initialization to DARTEL, whereas the alignment of the rest of the cortical morphology was induced only by the interpolation of the deformation between the sulci. Then, DARTEL refined the alignment of the cortical mantle but also of sulci since the initialization by DISCO solved most of the anatomical ambiguities.

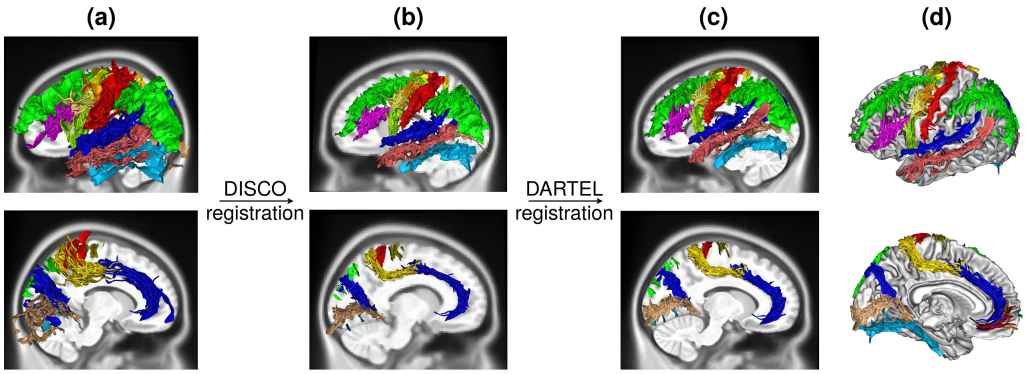

Fig. 5. Superimposition in the ICBM reference space, of all the sulci constraining the DISCO alignment before **(a)** DISCO, after **(b)** DISCO and **(c)** DISCO + DARTEL deformations; **(d)** all the sulci after the DISCO + DARTEL deformation shown on the mesh of white matter.

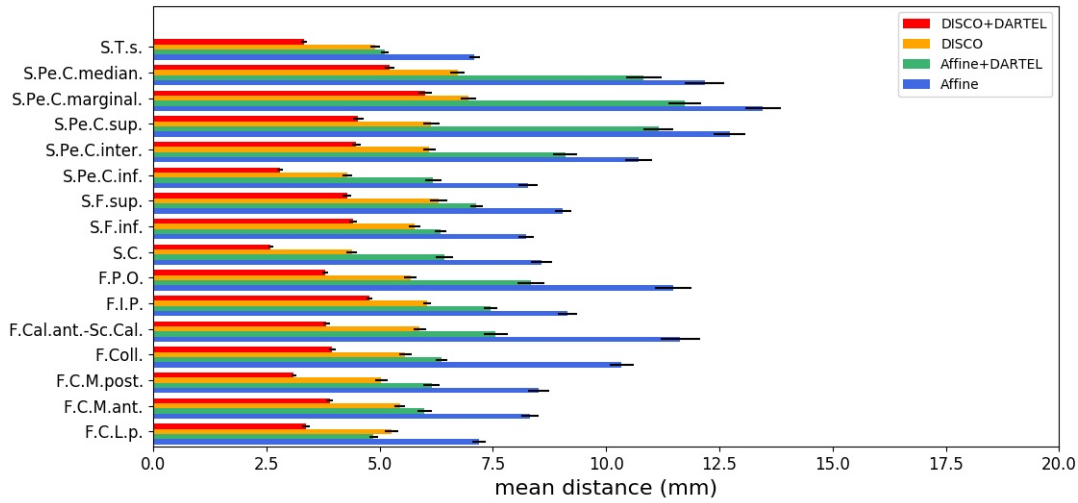

Fig. 6. Sulcal dispersion across the 14 brains. Average of the pairwise mean distance and its associated standard error of the mean (95% confidence interval) computed between each identical sulcal folds across the brains.

For each sulcus, we also studied the quality of alignment obtained by the different strategies using average pairwise distances (see Figure 6). This study highlights the improvement obtained with constraints compared with affine alignment (-41% on average for all selected sulci, significant difference between pairwise distances ($p < 5 \times 10^{-2}$)). It is also evident that DARTEL's initialization by DISCO preserves the alignment of the preselected sulci, and leads to a much better alignment than when only affine initialization is used (-45% on average for all sulci, significant difference between pairwise distances ($p < 5 \times 10^{-2}$)). These results are consistent with our previous observations (Lebenberg et al., 2018), which confirmed that without local initialization with DISCO, DARTEL does not always align the corresponding sulci. Finally, it is important to note the complementary nature of the two algorithms. Although DISCO enables a good matching of the selected sulci, DARTEL allows them to be finely deformed to align their shape details. Compared with DISCO alone, DISCO+DARTEL achieves an average improvement of 30% (significant difference between pairwise distances ($p < 5 \times 10^{-2}$)).

Atlas evaluation and comparison

Using a method of surface projection introduced in the context of the HBP (Mangin et al., 2021), the cytoarchitectonic maximum probability maps were projected onto the FreeSurfer-based surface mesh of the ICBM152casym white matter, with and without inflation, at "fsaverage" resolution (163842 vertices), as shown in Figure 7a, b. The area labels can be found in the 3D atlas viewer siibra-explorer. The Julich-Brain atlas version 3.0 (Amunts et al., 2020) was projected onto the same meshes. A visual comparison between our atlas and the standard Julich-Brain atlas is shown in Figure 8a, b. It can be observed that the maximum probability projections of the sensorimotor areas (4a, 4p, 3a, 3b and 1) (Geyer et al., 1996, 1999, 2000) of our atlas have a systematically elongated organization following the direction of the central sulcus, whereas this property observed in individual histological sections is not apparent in the Julich-Brain atlas projection released so far.

If we consider the maximum probability projection of each area as its proxy in the reference space, the shape and

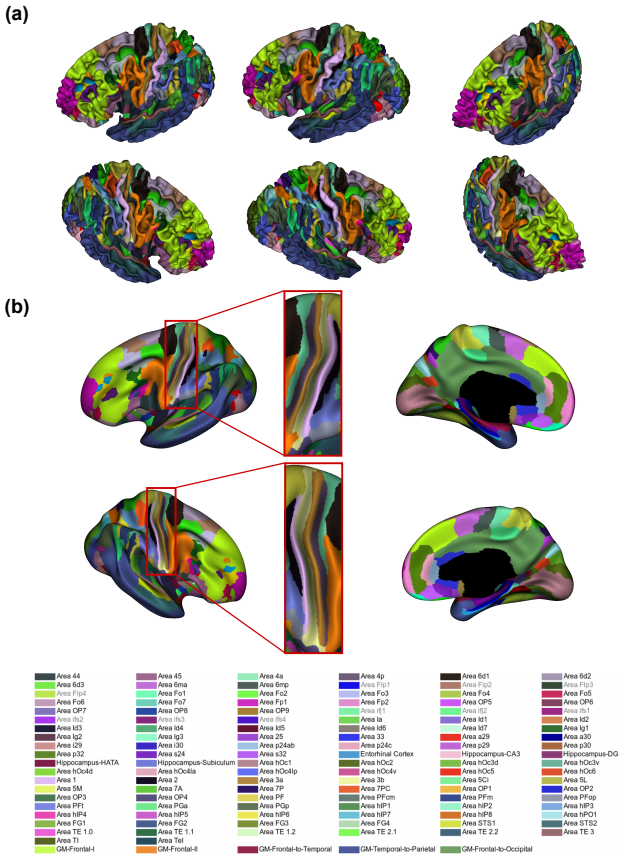

Fig. 7. DISCO + DARTEL cytoarchitectonic atlas projection on the ICBM152casym (a) white matter meshes (1st and 2nd rows correspond to the left and right hemispheres respectively; the three columns are different views to view the bottom of the sensorimotor areas better.) and (b) inflated white matter meshes.

localization of this proxy also reveal relationships with the gross features of the central sulcus that are maintained in individual brains, despite considerable inter-individual (and interhemispheric) variation in the superficial appearance of the central sulcus. Area 3a is located in the fundus of the central sulcus, and area 3b is located in the posterior bank of the central sulcus (Geyer et al., 1999, 2000). Area 1 occupies the crown of the postcentral gyrus and reaches down into the postcentral sulcus (Geyer et al., 1999, 2000). Area 4p lies in the lower part of the anterior bank of the central sulcus (Geyer et al., 1996), while area 4a occupies the higher part of the bank and extends beyond the gyral crest of the precentral gyrus in the upper part of the brain (White et al., 1997). Thus, while the posterior border of area 3b remains near the postcentral gyrus crest, the position of the anterior border of area 4a varies significantly according to the morphological features. Proceeding inferiorly toward the lateral fissure, the anterior border of area 4a withdraws posteriorly and recedes from the crest of the precentral gyrus to the depths of the central sulcus, as in individual brains (White et al., 1997). In addition, as observed in each of 40 hemispheres examined in histological sections, area 3 (a and b merged) extends approximately 1 cm beyond the lower limit of area 4 (p and a merged) and ends near the inferior terminus of the central sulcus (White et al., 1997). Most of these properties are diluted and do not appear on the MPMs, due to the greater fuzziness of the probabilistic maps and lack of control over the alignment of the central sulci. It is more difficult to compare the two versions in the associative parts of the brain, where the links between folding and architectonics are complex.

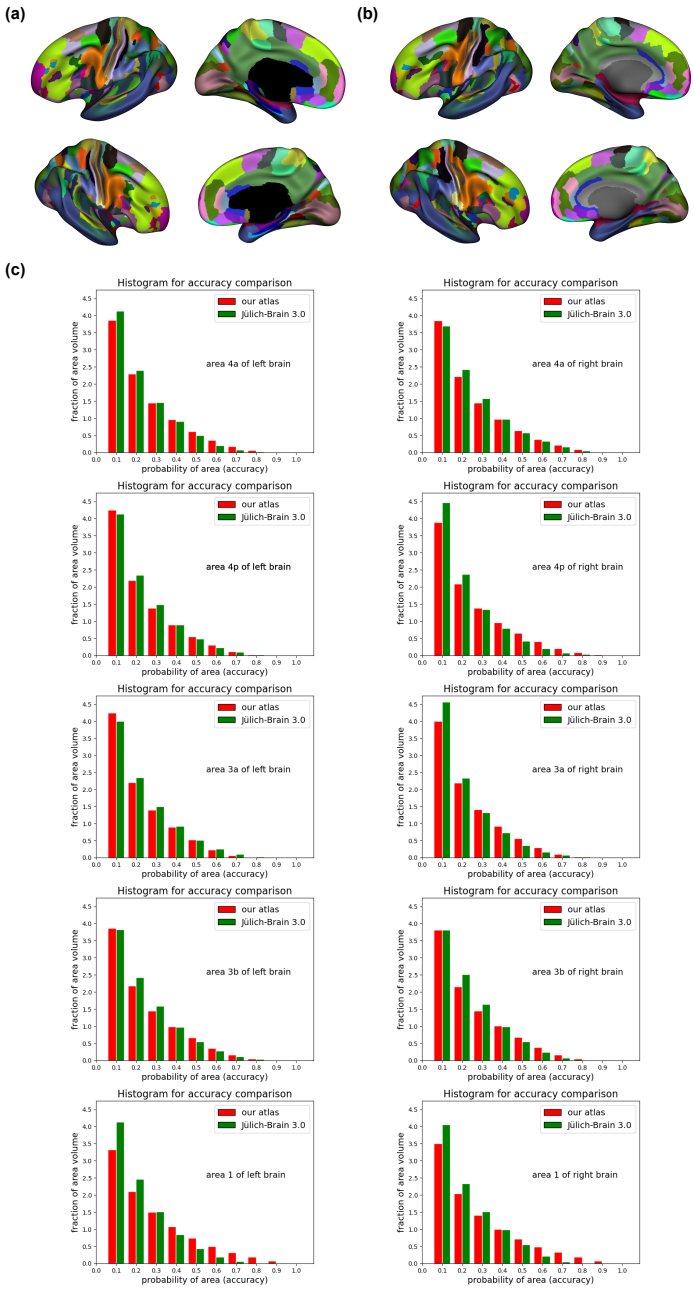

Fig. 8. Comparison of (a) our DISCO + DARTEL cytoarchitectonic atlas and (b) Julich-Brain atlas (Amunts et al., 2020) (version 3.0) in the ICBM152casym space; (c) histograms of the areal accuracy of our atlas and the Julich-Brain 3.0 atlas for the sensorimotor areas (4a, 4p, 3a, 3b and 1) of the left and right hemispheres. (a) and (b) are surface-based, whereas (c) is voxel-based.

In order to characterize the improvements observed in sensorimotor areas regarding the MPMs better, we sought to avoid the additional complexity induced by projection onto the

cortical surface. For each of the five sensorimotor areas in both hemispheres (Geyer et al., 1996, 1999, 2000), we computed the histograms for each nonzero voxel of the probability map in the ICBM152casym space, as shown in Figure 8c. Note that these probabilities can take only 10 values corresponding to the number of brains among the 10 contributing to a voxel. Then, the bar corresponding to $0.n$ provides the number of voxels covered by at least n brains normalized by the average volume occupied by the area in these 10 brains. Regardless of the area, the normalized number of voxels covered by at least five brains is always larger when using our alignment method, suggesting a better overlap of the underlying area across the brains. The only area with a similar overlap for both approaches is left 3a.

In addition, for all the areas except the Gap Maps, we show the differences in the fractions of area volume including at least five brains, projected onto the cortical surface mesh, as shown in Figure 9. Cortical regions benefiting from a large number of sulcal constraints during the DISCO alignment have a better overlap across the brains: in addition to the areas around the central sulcus (S.C.), some other areas such as those around the calcarine fissure (F.Cal.ant.-Sc.Cal.), the cingulate sulcus (or calloso-marginal fissure, F.C.M.) and the superior temporal sulcus (S.T.s.). However, the areas ventral to the intraparietal sulcus (F.I.P.) as well as the inferior frontal lobe performed poorly, possibly because of the lack of sulcal constraints in these regions during the alignment. Due to the considerable variability in folding patterns in these regions, we have not yet attempted to impose additional sulcal constraints. A preliminary study on the links between folding patterns and architectonics in these regions has shown that it was difficult to identify unambiguous landmarks in the inferior parietal lobule (Caspers et al., 2006).

An illustration of the difficulty for Brodmann areas is shown in Figure 10. For each left hemisphere of the 10 brains, we visualized the relationship between Brodmann areas 44 and 45 and the precentral, diagonal and inferior frontal sulci, using a dedicated browser of the BrainVISA package (Rivière et al., 2022). It can be observed that the area 44 is limited posteriorly by the diagonal sulcus in some brains (brains 1 and 7), by the precentral sulcus in others (brains 2, 4, 5, 8 and 10) and even seems to go a bit beyond the level of the precentral sulcus in a few more (brains 3, 6 and 9). We have to clarify whether this variability is related to a misunderstanding of the variability in the folding pattern, or to the existence of different configurations in the general population.

DISCUSSION AND CONCLUSION

The segregation of the cortical mantle into different areas, highlighted by cytoarchitectonics, is a fundamental feature of the human brain. It provides a structural basis for the specialization of different brain regions. Areas highlighted by cytoarchitectonics are often associated with specific functions, such as sensory perception, motor control, language processing, and higher cognitive functions. To compensate for the fact that this information is currently not accessible in vivo, the postmortem histological mapping has been integrated into neuroimaging pipelines thanks to the spatial normalization paradigm. However, the concept of spatial normalization is relatively vague (Mangin et al., 2016) and covers various methods for cross-brain alignment. In this study, we demonstrate that the strategy adopted thus far is suboptimal and can be improved by using explicit landmarks derived from cortical folding.

It is possible to improve the superposition of individual postmortem architectural maps by controlling the alignment of the selected sulci. This result was expected in the sensorimotor region, where the bottom of the central sulcus is known to correspond to the boundary between the sensory and motor areas, and in general, in all primary areas for similar reasons (Fischl et al., 2008). However, this improvement is also notable in some regions where the link between folding and architectonics is more complex (areas systematically buried in a particular sulcus without necessarily reaching its bottom, areas systematically localized in a gyrus, etc.). This kind of relationship has been described for instance relative to the cingulate sulcus (Ronan et al., 2020; Palomero-Gallagher et al., 2019), which is one of our landmarks, and the architectonic superposition in our new atlas has been improved. However, in some associative regions where the variability of folding patterns is massive, our method degraded the quality of superimpositions, probably because we were unable to define reliable landmarks in terms of the relationship between folding and architectural area topography, or because the link between anatomy and cytoarchitecture in these regions is arguable. For example, Figure 10 shows that our use of the inferior precentral sulcus as a landmark is questionable and probably degraded the quality of the architectonic superposition with regard to Broca's areas. According to the sulcus labelling proposed in this figure (and Supplementary Figure 12 without architectonic areas), the position of this sulcus relative to area 44 is not stable. But this sulcus automatic labelling could be wrong in some subjects: for instance, in subjects 3, 6, and 9, the fold labelled inferior precentral sulcus (in green) could in fact be the diagonal sulcus, which was the initial choice of the anatomists, who performed the cytoarchitectonic mapping (Amunts et al., 2004). The supplementary figure 13 illustrates this alternative labelling. It seems that the inferior precentral sulcus identified by the anatomists in the histological sections is missing in the skeleton-based representation extracted by our complex pipeline, which led to a failure of the fold automatic delineation in the cortex negative skeleton, leading to wrong sulcus annotation.

The difficulties in Broca's area originate in part from the considerable variability in the folding patterns in this region. The anterior ramus (F.C.L.r.ant) of the lateral fissure (F.C.L.) is a characteristic sulcus that forms the morphological boundary between the pars triangularis and pars orbitalis of the inferior frontal gyrus (Keller et al., 2009; Sprung-Much and Petrides, 2020). It is often considered to mark the anterior border of area 45 (Keller et al., 2009; Amunts et al., 2010). The ascending ramus (F.C.L.r.asc) extends dorsally from the lateral fissure, separating the pars opercularis from the pars triangularis of the inferior frontal gyrus (Keller et al., 2009; Sprung-Much and Petrides, 2018). It is often considered to mark the border between areas 44 and 45 (Keller et al., 2009; Amunts et al., 2010). The inferior precentral sulcus (S.Pe.C.inf) is the morphological posterior boundary of the pars opercularis and is often considered to mark the posterior border of area 44 (Keller et al., 2009; Amunts et al., 2010). However, studies on the relationship between macroscopic morphological features and the border between these two areas have reported low correspondence (Amunts et al., 1999; Fischl et al., 2008). Therefore, the map of the region proposed by Brodmann is only a schematic 2-D sketch that does not account for inter-subject or inter-hemispheric variability (Amunts et al., 2010).

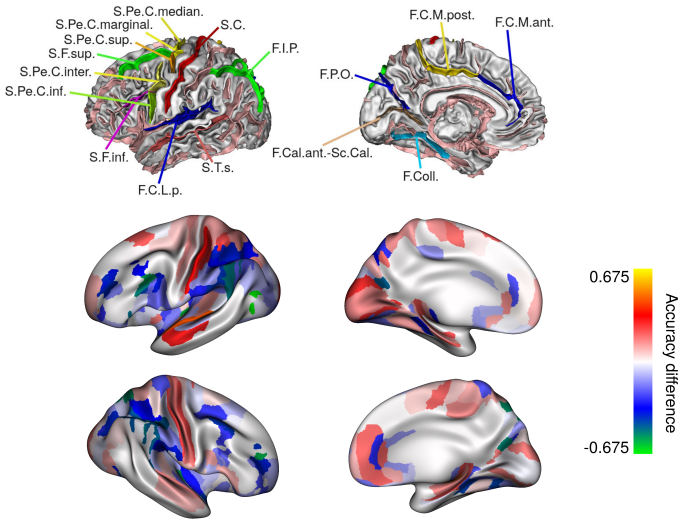

Fig. 9. Differences in volume with at least 5 brains overlapping (our atlas − Julich-Brain atlas (version 3.0)) for each cytoarchitectonic area projected on the ICBM152casym inflated white matter mesh.

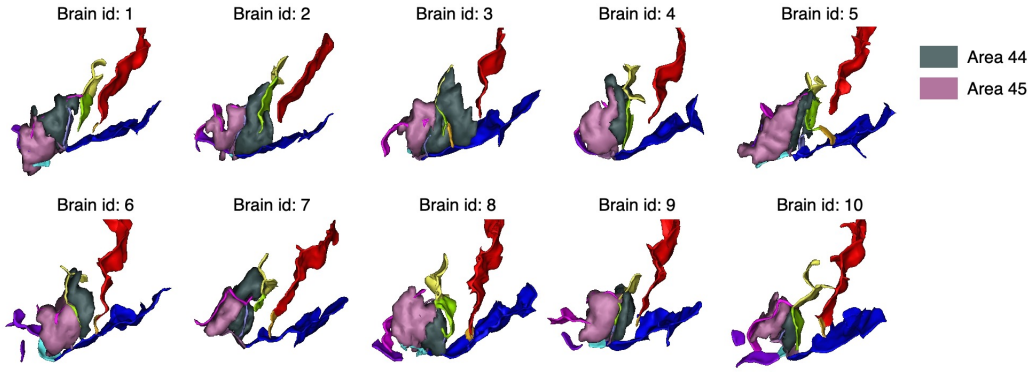

Fig. 10. Relationship between cytoarchitectonic areas 44, 45 and the surrounding sulci for the left hemispheres of the first 10 Jülich brains. Note that the sulcus recognition results from an automatic process trained from in vivo MRI that could be wrong in some places.

Furthermore, the frequent presence of additional folds in this area leads to ambiguities when labeling the sulci: additional branches of the lateral fissure, such as the sulcus diagonalis (F.C.L.r.diag.) can be observed in half of the subjects (Sprung-Much and Petrides, 2018, 2020), and additional folds in the precentral gyrus such as the S.C.sylvian, impede the identification of the inferior precentral sulcus (Eichert et al., 2021). In addition, the various interruption patterns of the inferior frontal sulcus (S.F.inf.), which provides additional morphological boundaries to the region, are difficult to decipher (Ruland et al., 2022). Finally, adapting MRI-based sulcus detection tools to histological images is likely to create artifacts (missing or spurious folds) that impede labeling. The automatic labeling of the folds in this region obtained for the 10 subjects with architectonic mapping of areas 44 and 45 is shown in Supplementary Figure 12, and illustrates the difficulty in unambiguously defining folding landmarks in Brodmann areas, probably even for the inferior precentral sulcus because of failures of our preprocessing.

It should be noted that while Dartel does not provide any control of the alignment of sulci, the preliminary results show that we manage to control this alignment for the landmarks thanks to the initial alignment provided by Disco but also because we tune the Dartel parameters to regularize the deformation field. It means that the local arrangement of sulci relatively to each other is preserved in each individual. It does not mean that Dartel has the ability to match incompatible folding patterns, but it means that in each area, the most consensual folding pattern across the 14 brains is probably selected thanks to the group level alignment performed by DISCO. An interesting further development would be to compare this result with the result achieve with an alternative software, for instance Ants. In regions without any sulcus-based constraint, it could appear that some framework provide more efficient alignment relative to the underlying link between folding and architectonic.

The biological processes that cause the cortex to fold during development have not yet been characterized, but today, they are the subject of considerable research (Llinares-Benadero and Borrell, 2019). Various physical models have been proposed (Toro and Burnod, 2005; Bayly et al., 2013; Tallinen et al., 2014; Kroenke and Bayly, 2018; Wang et al., 2019, 2021), the most recent of which models different layers in which neurons are generated, including the outer subventricular zone (Zarzor

et al., 2023). A recurring idea is that the tangential growth of the outer layer of the brain, which is far superior to that of the white matter, necessitates folding. The simulation of this model from a smooth fetal cortical surface leads to folds whose geometry closely resembles that of mammalian cortices (Tallinen et al., 2016); however, the patterns and orientation of folds differ from actual brains. For the folding pattern to correspond to the stereotypical template of a given species, spatial heterogeneity needs to be introduced into such models to impose a global pattern that is recurrent across individuals. Several explanations for this heterogeneity have been proposed. The existence of a protomap of primary folds and gyri of genetic origin in the ventricular zone, linked to heterogeneous patterning of gene expression, is today a strong biological model (Kriegstein et al., 2006; Borrell and Calegari, 2014; de Juan Romero et al., 2015; Borrell, 2018). Differences in neuropil development linked to the chronology of maturation of different architectural areas (Rash et al., 2023), or even a contribution from tensions created by axon bundles (Essen, 1997), could be complementary causal processes, maybe related to secondary or tertiary folding. A very different hypothesis is that nature exploits the geometry of the cortical folding pattern to optimize the layout of architectonic areas once the folds have been established from purely mechanical processes, for example in terms of connectivity (Foubet et al., 2019; Heuer and Toro, 2019).

All these models, which could each contribute, suggest a close but probably complex link between cytoarchitectural subdivisions and cortical folding patterns. Note that we could even assume that the protomap of primary folds is linked to the protomap of architectonic areas (Rakic, 1988). It therefore seems important to seek to use cortical folding as a proxy for architectonic area topography, as proposed in this article. This point of view is relatively consensual for primary areas and is relatively easy to implement because of the stability of the cortical folding patterns observed there. In associative areas, the situation is complicated by the inter-individual variability in local folding patterns. Several studies are now seeking to map alternative local patterns in the general population (Sun et al., 2007; Plaze et al., 2015; Sprung-Much and Petrides, 2018; Cachia et al., 2018; Snyder et al., 2019; Duan et al., 2019; Chavas et al., 2022; Troiani et al., 2022). These alternative patterns are often linked to the interruption of large furrows by small gyri, which are usually buried, and probably have a specific architectural meaning (Mangin et al., 2019). The aim of this field of research is either to devise a method for defining the notion of gyration anomalies potentially associated with developmental abnormalities in architectonics (Guillon et al., 2021), or to stratify the population into groups of subjects with different architectonic topographies, so as to perform stratified group analyses of neuroimaging data (Sun et al., 2016; Guevara et al., 2022). These studies show that using sulci as landmarks may require a different choice depending on the local folding pattern. The number of brains endowed with histology-based architectural mapping is probably too limited for the stratification strategy. Therefore, to further improve the transfer of architectonic mapping to subjects of in vivo neuroimaging experiments, a complementary proxy derived from functional mappings should be used in the spirit of the proposal of Glasser et al. relative to fMRI imaging (Glasser et al., 2016).

This study is a milestone in a long-term research program aimed at improving the bridge that enables postmortem architectonic information to be used by in vivo neuroimaging studies in the most efficient way. In the future, the joint use of resting-state functional MRI should make it possible to add new constraints to the alignment process. The tools described in this paper will be integrated into the EBRAINS research infrastructure to enable their use by communities. Our aim will be to enable research groups proposing nomenclatures for annotating secondary and tertiary sulci (Voorhies et al., 2021; Amiez et al., 2023; Weiner, 2023) to apply them to postmortem Jülich brains, and then to access a benchmark quantifying the ability of their nomenclature to predict the variability of the location of architectonic areas. To achieve this goal, however, we need first to improve the quality of the fold representations extracted from histological images.

FUNDING

This work was supported by the European Union's Horizon 2020 Research and Innovation Programme under Grant Agreement No. 945539 (HBP SGA3), and by the ANR-20-CHIA-0027-01 FOLDDICO.

AUTHOR CONTRIBUTIONS

Xiaoyu Wang, Yann Leprince and Jessica Lebenberg developed the tools, conceived the experiments and performed data analysis. Katrin Amunts provided anatomical expertise. Xiaoyu Wang and Jean-François Mangin drafted the manuscript. Jean-François Mangin and Denis Rivière supervised the project. All the authors edited and approved the final version of the manuscript.

CONFLICT OF INTEREST

The authors declare no conflict of interest.

References

Alkemade, A., Pine, K., Kirilina, E., Keuken, M. C., Mulder, M. J., Balesar, R., Groot, J. M., Bleys, R. L., Trampel, R., Weiskopf, N., et al. (2020). 7 tesla mri followed by histological 3d reconstructions in whole-brain specimens. *Front Neuroanat*, page 68.

Amiez, C., Sallet, J., Giacometti, C., Verstraete, C., Gandaux, C., Morel-Latour, V., Meguerditchian, A., Hadj-Bouziane, F., Ben Hamed, S., Hopkins, W. D., et al. (2023). A revised perspective on the evolution of the lateral frontal cortex in primates. *Sci Adv*, 9(20):eadf9445.

Amunts, K., Lenzen, M., Friederici, A. D., Schleicher, A., Morosan, P., Palomero-Gallagher, N., and Zilles, K. (2010). Broca's region: novel organizational principles and multiple receptor mapping. *PLoS Biol*, 8(9):e1000489.

Amunts, K., Lepage, C., Borgeat, L., Mohlberg, H., Dickscheid, T., Rousseau, M.-É., Bludau, S., Bazin, P.-L., Lewis, L. B., Oros-Peusquens, A.-M., et al. (2013). Bigbrain: an ultrahigh-resolution 3d human brain model. *science*, 340(6139):1472–1475.

Amunts, K., Mohlberg, H., Bludau, S., and Zilles, K. (2020). Julich-brain: A 3d probabilistic atlas of the human brain's cytoarchitecture. *Science*, 369(6506):988–992.

Amunts, K., Schleicher, A., Bürgel, U., Mohlberg, H., Uylings, H. B., and Zilles, K. (1999). Broca's region revisited: cytoarchitecture and intersubject variability. *J Comp Neurol*, 412(2):319–341.

Amunts, K., Weiss, P. H., Mohlberg, H., Pieperhoff, P., Eickhoff, S., Gurd, J. M., Marshall, J. C., Shah, N. J., Fink, G. R., and Zilles, K. (2004). Analysis of neural mechanisms underlying verbal fluency in cytoarchitectonically defined stereotaxic space—the roles of brodmann areas 44 and 45. *Neuroimage*, 22(1):42–56.

Amunts, K. and Zilles, K. (2015). Architectonic mapping of the human brain beyond brodmann. *Neuron*, 88(6):1086–1107.

Ashburner, J. (2007). A fast diffeomorphic image registration algorithm. *Neuroimage*, 38(1):95–113.

Auzias, G., Colliot, O., Glaunes, J. A., Perrot, M., Mangin, J.-F., Trouve, A., and Baillet, S. (2011). Diffeomorphic brain registration under exhaustive sulcal constraints. *IEEE TMI*, 30(6):1214–1227.

Bayly, P., Okamoto, R., Xu, G., Shi, Y., and Taber, L. (2013). A cortical folding model incorporating stress-dependent growth explains gyral wavelengths and stress patterns in the developing brain. *Phys Biol*, 10(1):016005.

Borrell, V. (2018). How cells fold the cerebral cortex. *J Neurosci*, 38(4):776–783.

Borrell, V. and Calegari, F. (2014). Mechanisms of brain evolution: regulation of neural progenitor cell diversity and cell cycle length. *Neurosci Res*, 86:14–24.

Cachia, A., Roell, M., Mangin, J.-F., Sun, Z. Y., Jobert, A., Braga, L., Houde, O., Dehaene, S., and Borst, G. (2018). How interindividual differences in brain anatomy shape reading accuracy. *Brain Struct Funct*, 223:701–712.

Caspers, S., Geyer, S., Schleicher, A., Mohlberg, H., Amunts, K., and Zilles, K. (2006). The human inferior parietal cortex: cytoarchitectonic parcellation and interindividual variability. *Neuroimage*, 33(2):430–448.

Chavas, J., Guillon, L., Pascucci, M., Dufumier, B., Rivière, D., and Mangin, J.-F. (2022). Unsupervised representation learning of cingulate cortical folding patterns. In *International Conference on Medical Image Computing and Computer-Assisted Intervention*, pages 77–87. Springer.

Cointepas, Y., Mangin, J.-F., Garnero, L., Poline, J.-B., and Benali, H. (2001). Brainvisa: software platform for visualization and analysis of multi-modality brain data. *Neuroimage*, 13(6):98.

de Juan Romero, C., Bruder, C., Tomasello, U., Sanz-Anquela, J. M., and Borrell, V. (2015). Discrete domains of gene expression in germinal layers distinguish the development of gyrencephaly. *EMBO J*, 34(14):1859–1874.

Dice, L. R. (1945). Measures of the amount of ecologic association between species. *Ecology*, 26(3):297–302.

Duan, D., Xia, S., Rekik, I., Meng, Y., Wu, Z., Wang, L., Lin, W., Gilmore, J. H., Shen, D., and Li, G. (2019). Exploring folding patterns of infant cerebral cortex based on multi-view curvature features: Methods and applications. *Neuroimage*, 185:575–592.

Eichert, N., Watkins, K. E., Mars, R. B., and Petrides, M. (2021). Morphological and functional variability in central and subcentral motor cortex of the human brain. *Brain Struct Funct*, 226(1):263–279.

Eickhoff, S. B., Heim, S., Zilles, K., and Amunts, K. (2006). Testing anatomically specified hypotheses in functional imaging using cytoarchitectonic maps. *Neuroimage*, 32(2):570–582.

Eickhoff, S. B., Stephan, K. E., Mohlberg, H., Grefkes, C., Fink, G. R., Amunts, K., and Zilles, K. (2005). A new spm toolbox for combining probabilistic cytoarchitectonic maps and functional imaging data. *Neuroimage*, 25(4):1325–1335.

Essen, D. C. v. (1997). A tension-based theory of morphogenesis and compact wiring in the central nervous system. *Nat*, 385(6614):313–318.

Fischer, C., Operto, G., Laguitton, S., Perrot, M., Denghien, I., Rivière, D., and Mangin, J. (2012). Morphologist 2012: the new morphological pipeline of brainvisa. *Proc. HBM*.

Fischl, B., Rajendran, N., Busa, E., Augustinack, J., Hinds, O., Yeo, B. T., Mohlberg, H., Amunts, K., and Zilles, K. (2008). Cortical folding patterns and predicting cytoarchitecture. *Cereb Cortex*, 18(8):1973–1980.

Foubet, O., Trejo, M., and Toro, R. (2019). Mechanical morphogenesis and the development of neocortical organisation. *Cortex*, 118:315–326.

Geyer, S., Ledberg, A., Schleicher, A., Kinomura, S., Schormann, T., Bürgel, U., Klingberg, T., Larsson, J., Zilles, K., and Roland, P. E. (1996). Two different areas within the primary motor cortex of man. *Nature*, 382(6594):805–807.

Geyer, S., Schleicher, A., and Zilles, K. (1999). Areas 3a, 3b, and 1 of human primary somatosensory cortex: 1. microstructural organization and interindividual variability. *Neuroimage*, 10(1):63–83.

Geyer, S., Schormann, T., Mohlberg, H., and Zilles, K. (2000). Areas 3a, 3b, and 1 of human primary somatosensory cortex: 2. spatial normalization to standard anatomical space. *Neuroimage*, 11(6):684–696.

Glasser, M. F., Coalson, T. S., Robinson, E. C., Hacker, C. D., Harwell, J., Yacoub, E., Ugurbil, K., Andersson, J., Beckmann, C. F., Jenkinson, M., et al. (2016). A multi-modal parcellation of human cerebral cortex. *Nat*, 536(7615):171–178.

Glaunes, J., Trouvé, A., and Younes, L. (2004). Diffeomorphic matching of distributions: A new approach for unlabelled point-sets and sub-manifolds matching. In *Proceedings of the 2004 IEEE Computer Society Conference on Computer Vision and Pattern Recognition, 2004. CVPR 2004.*, volume 2, pages II–II. IEEE.

Guevara, M., Sun, Z.-Y., Guevara, P., Rivière, D., Grigis, A., Poupon, C., and Mangin, J.-F. (2022). Disentangling the variability of the superficial white matter organization using regional-tractogram-based population stratification. *NeuroImage*, 255:119197.

Guillon, L., Cagna, B., Dufumier, B., Chavas, J., Rivière, D., and Mangin, J.-F. (2021). Detection of abnormal folding patterns with unsupervised deep generative models. In *International Workshop on Machine Learning in Clinical Neuroimaging*, pages 63–72. Springer.

Heuer, K. and Toro, R. (2019). Role of mechanical morphogenesis in the development and evolution of the neocortex. *Phys Life Rev*, 31:233–239.

Hömke, L. (2006). A multigrid method for anisotropic pdes in elastic image registration. *Numer Linear Algebra Appl*, 13(2-3):215–229.

Kabdebon, C., Leroy, F., Simmonet, H., Perrot, M., Dubois, J., and Dehaene-Lambertz, G. (2014). Anatomical correlations of the international 10–20 sensor placement system in infants. *Neuroimage*, 99:342–356.

Keller, S. S., Crow, T., Foundas, A., Amunts, K., and Roberts, N. (2009). Broca's area: nomenclature, anatomy, typology and asymmetry. brain and language. *Brain Lang*, 109(1):29–48.

Klein, A., Andersson, J., Ardekani, B. A., Ashburner, J., Avants, B., Chiang, M.-C., Christensen, G. E., Collins, D. L., Gee, J., Hellier, P., et al. (2009). Evaluation of 14 nonlinear deformation algorithms applied to human brain mri

registration. *Neuroimage*, 46(3):786–802.

Kriegstein, A., Noctor, S., and Martínez-Cerdeño, V. (2006). Patterns of neural stem and progenitor cell division may underlie evolutionary cortical expansion. *Nat Rev Neurosci*, 7(11):883–890.

Kroenke, C. D. and Bayly, P. V. (2018). How forces fold the cerebral cortex. *J Neurosci*, 38(4):767–775.

Lebenberg, J., Labit, M., Auzias, G., Mohlberg, H., Fischer, C., Rivière, D., Duchesnay, E., Kabdebon, C., Leroy, F., Labra, N., et al. (2018). A framework based on sulcal constraints to align preterm, infant and adult human brain images acquired in vivo and post mortem. *Brain Struct Funct*, 223(9):4153–4168.

Leprince, Y., Stochino, A., Foubet, O., Hopkins, W. D., and Mangin, J.-F. (2020). The morphological evolution of the primate brain revealed by alignment of the cortical sulci. In *OHBM 2020-26th Annual Meeting of the Organization for Human Brain Mapping*.

Llinares-Benadero, C. and Borrell, V. (2019). Deconstructing cortical folding: genetic, cellular and mechanical determinants. *Nat Rev Neurosci*, 20(3):161–176.

Mangin, J.-F., Le Guen, Y., Labra, N., Grigis, A., Frouin, V., Guevara, M., Fischer, C., Rivière, D., Hopkins, W. D., Régis, J., et al. (2019). "plis de passage" deserve a role in models of the cortical folding process. *Brain Topogr*, 32:1035–1048.

Mangin, J.-F., Lebenberg, J., Lefranc, S., Labra, N., Auzias, G., Labit, M., Guevara, M., Mohlberg, H., Roca, P., Guevara, P., et al. (2016). Spatial normalization of brain images and beyond. *Med Image Anal*, 33:127–133.

Mangin, J.-F., Rivière, D., and Amunts, K. (2021). Surface projections of julich-brain cytoarchitectonic maps.

Palomero-Gallagher, N., Hoffstaedter, F., Mohlberg, H., Eickhoff, S. B., Amunts, K., and Zilles, K. (2019). Human pregenual anterior cingulate cortex: structural, functional, and connectional heterogeneity. *Cereb Cortex*, 29(6):2552–2574.

Passingham, R. E., Stephan, K. E., and Kötter, R. (2002). The anatomical basis of functional localization in the cortex. *Nat Rev Neurosci*, 3(8):606–616.

Perrot, M., Rivière, D., and Mangin, J.-F. (2011). Cortical sulci recognition and spatial normalization. *Med Image Anal*, 15(4):529–550.

Plaze, M., Mangin, J.-F., Paillère-Martinot, M.-L., Artiges, E., Olié, J.-P., Krebs, M.-O., Gaillard, R., Martinot, J.-L., and Cachia, A. (2015). "who is talking to me?"—self–other attribution of auditory hallucinations and sulcation of the right temporoparietal junction. *Schizophr Res*, 169(1-3):95–100.

Rakic, P. (1988). Specification of cerebral cortical areas. *Science*, 241(4862):170–176.

Rash, B. G., Arellano, J. I., Duque, A., and Rakic, P. (2023). Role of intracortical neuropil growth in the gyrification of the primate cerebral cortex. *PNAS*, 120(1):e2210967120.

Rivière, D., Leprince, Y., Labra, N., Vindas, N., Foubet, O., Cagna, B., Loh, K. K., Hopkins, W., Balzeau, A., Mancip, M., et al. (2022). Browsing multiple subjects when the atlas adaptation cannot be achieved via a warping strategy. *Front Neuroinform*, 16:7.

Ronan, L., Alexander-Bloch, A., and Fletcher, P. C. (2020). Childhood obesity, cortical structure, and executive function in healthy children. *Cereb Cortex*, 30(4):2519–2528.

Ruland, S. H., Palomero-Gallagher, N., Hoffstaedter, F., Eickhoff, S. B., Mohlberg, H., and Amunts, K. (2022). The inferior frontal sulcus: cortical segregation, molecular architecture and function. *Cortex*, 153:235–256.

Snyder, W., Patti, M., and Troiani, V. (2019). An evaluation of automated tracing for orbitofrontal cortex sulcogyral pattern typing. *J Neurosci Methods*, 326:108386.

Sprung-Much, T. and Petrides, M. (2018). Morphological patterns and spatial probability maps of two defining sulci of the posterior ventrolateral frontal cortex of the human brain: the sulcus diagonalis and the anterior ascending ramus of the lateral fissure. *Brain Struct Funct*, 223:4125–4152.

Sprung-Much, T. and Petrides, M. (2020). Morphology and spatial probability maps of the horizontal ascending ramus of the lateral fissure. *Cereb Cortex*, 30(3):1586–1602.

Sun, Z., Pinel, P., Rivière, D., Moreno, A., Dehaene, S., and Mangin, J.-F. (2016). Linking morphological and functional variability in hand movement and silent reading. *Brain Struct Funct*, 221:3361–3371.

Sun, Z. Y., Rivière, D., Poupon, F., Régis, J., and Mangin, J. F. (2007). Automatic inference of sulcus patterns using 3d moment invariants. In *Medical Image Computing and Computer-Assisted Intervention–MICCAI 2007: 10th International Conference, Brisbane, Australia, October 29-November 2, 2007, Proceedings, Part I 10*, pages 515–522. Springer.

Tallinen, T., Chung, J. Y., Biggins, J. S., and Mahadevan, L. (2014). Gyrification from constrained cortical expansion. *PNAS*, 111(35):12667–12672.

Tallinen, T., Chung, J. Y., Rousseau, F., Girard, N., Lefèvre, J., and Mahadevan, L. (2016). On the growth and form of cortical convolutions. *Nat Phys*, 12(6):588–593.

Toro, R. and Burnod, Y. (2005). A morphogenetic model for the development of cortical convolutions. *Cereb Cortex*, 15(12):1900–1913.

Troiani, V., Snyder, W., Kozick, S., Patti, M. A., and Beiler, D. (2022). Variability and concordance of sulcal patterns in the orbitofrontal cortex: A twin study. *Psychiatry Res Neuroimaging*, 324:111492.

Voorhies, W. I., Miller, J. A., Yao, J. K., Bunge, S. A., and Weiner, K. S. (2021). Cognitive insights from tertiary sulci in prefrontal cortex. *Nat Commun*, 12(1):5122.

Wang, X., Bohi, A., Al Harrach, M., Dinomais, M., Lefèvre, J., and Rousseau, F. (2019). On early brain folding patterns using biomechanical growth modeling. In *2019 41st Annual International Conference of the IEEE Engineering in Medicine and Biology Society (EMBC)*, pages 146–149. IEEE.

Wang, X., Lefèvre, J., Bohi, A., Harrach, M. A., Dinomais, M., and Rousseau, F. (2021). The influence of biophysical parameters in a biomechanical model of cortical folding patterns. *Sci Rep*, 11(1):7686.

Wei, Y., Scholtens, L. H., Turk, E., and Van Den Heuvel, M. P. (2018). Multiscale examination of cytoarchitectonic similarity and human brain connectivity. *Netw Neurosci*, 3(1):124–137.

Weiner, K. S. (2023). The hypothesis of fundal cognition. *Nat Rev Neurosci*, 24(9):521–521.

White, L., Andrews, T., Hulette, C., Richards, A., Groelle, M., Paydarfar, J., and Purves, D. (1997). Structure of the human sensorimotor system. i: Morphology and cytoarchitecture of the central sulcus. *Cereb Cortex (New York, NY: 1991)*, 7(1):18–30.

Yassa, M. A. and Stark, C. E. (2009). A quantitative evaluation of cross-participant registration techniques for mri studies of the medial temporal lobe. *Neuroimage*, 44(2):319–327.

Zachlod, D., Palomero-Gallagher, N., Dickscheid, T., and Amunts, K. (2023). Mapping cytoarchitectonics and receptor architectonics to understand brain function and connectivity. *Biol Psychiatry*, 93(5):471–479.

Zarzor, M. S., Blumcke, I., and Budday, S. (2023). Exploring the role of the outer subventricular zone during cortical folding through a physics-based model. *Elife*, 12:e82925.

SUPPLEMENTARY

Table 1. Brains used for the alignment and atlas generation.

Brain id	Gender	Age	Fresh weight (g)	Pathology
1	Female	79	1350	Carcinoma of the bladder
2	Male	56	1270	Rectal cancer
3	Male	69	1360	Multiple cerebral infarctions
4	Male	75	1349	Toxic glomerulonephritis
5	Female	59	1142	Cardiorespiratory insufficiency
6	Male	54	1757	Myocardial infarction
7	Male	37	1437	Cardiac arrest
8	Female	72	1216	Kidney failure, status spongiosus
9	Female	79	1110	Arteriosclerosis, basal ganglia infarction
10	Female	85	1046	Mesenteric artery infarction
11	Male	74	1381	Myocardial infarction
12	Female	43	1198	Cor pulmonale, recurrence, pulmonary embolism
13	Male	39	1234	Drowning
14	Female	86	1113	Cardiorespiratory insufficiency

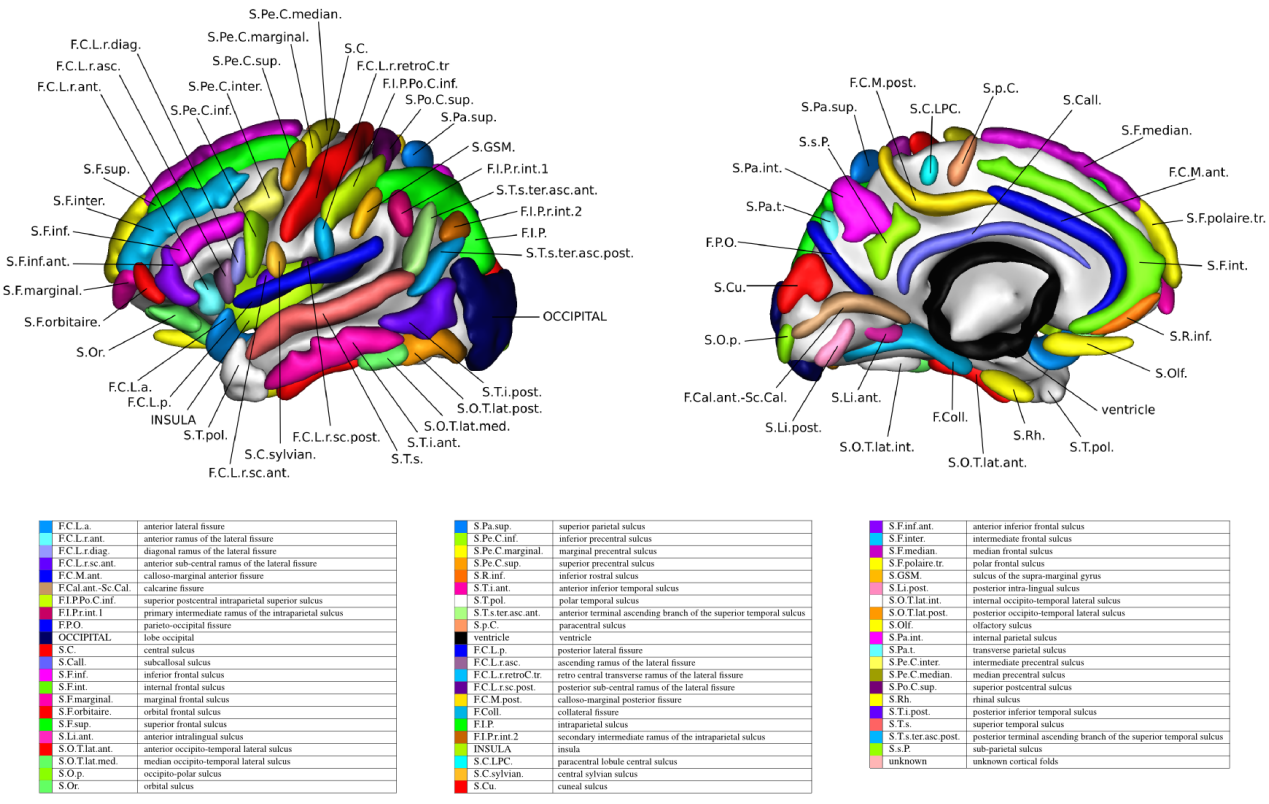

F.C.L.a.	anterior lateral fissure
F.C.L.r.ant.	anterior ramus of the lateral fissure
F.C.L.r.diag.	diagonal ramus of the lateral fissure
F.C.L.r.sc.ant.	anterior sub-central ramus of the lateral fissure
F.C.M.ant.	calloso-marginal anterior fissure
F.Cal.ant.-Sc.Cal.	calcarine fissure
F.I.P.Po.C.inf.	superior postcentral intraparietal superior sulcus
F.I.P.r.int.1	primary intermediate ramus of the intraparietal sulcus
F.P.O.	parieto-occipital fissure
OCCIPITAL	lobe occipital
S.C.	central sulcus
S.Call.	subcallosal sulcus
S.F.inf.	inferior frontal sulcus
S.F.int.	internal frontal sulcus
S.F.marginal.	marginal frontal sulcus
S.F.orbitaire.	orbital frontal sulcus
S.F.sup.	superior frontal sulcus
S.Li.ant.	anterior intralingual sulcus
S.O.T.lat.ant.	anterior occipito-temporal lateral sulcus
S.O.T.lat.med.	median occipito-temporal lateral sulcus
S.O.p.	occipito-polar sulcus
S.Or.	orbital sulcus

S.Pa.sup.	superior parietal sulcus
S.Pe.C.inf.	inferior precentral sulcus
S.Pe.C.marginal.	marginal precentral sulcus
S.Pe.C.sup.	superior precentral sulcus
S.R.inf.	inferior rostral sulcus
S.T.i.ant.	anterior inferior temporal sulcus
S.T.pol.	polar temporal sulcus
S.T.s.ter.asc.ant.	anterior terminal ascending branch of the superior temporal sulcus
S.p.C.	paracentral sulcus
ventricle	ventricle
F.C.L.p.	posterior lateral fissure
F.C.L.r.asc.	ascending ramus of the lateral fissure
F.C.L.r.retroC.tr.	retro central transverse ramus of the lateral fissure
F.C.L.r.sc.post.	posterior sub-central ramus of the lateral fissure
F.C.M.post.	calloso-marginal posterior fissure
F.Coll.	collateral fissure
F.I.P.	intraparietal sulcus
F.I.P.r.int.2	secondary intermediate ramus of the intraparietal sulcus
INSULA	insula
S.C.LPC.	paracentral lobule central sulcus
S.C.sylvian.	central sylvian sulcus
S.Cu.	cuneal sulcus

S.F.inf.ant.	anterior inferior frontal sulcus
S.F.inter.	intermediate frontal sulcus
S.F.median.	median frontal sulcus
S.F.polaire.tr.	polar frontal sulcus
S.GSM.	sulcus of the supra-marginal gyrus
S.Li.post.	posterior intra-lingual sulcus
S.O.T.lat.int.	internal occipito-temporal lateral sulcus
S.O.T.lat.post.	posterior occipito-temporal lateral sulcus
S.Olf.	olfactory sulcus
S.Pa.int.	internal parietal sulcus
S.Pa.t.	transverse parietal sulcus
S.Pe.C.inter.	intermediate precentral sulcus
S.Pe.C.median.	median precentral sulcus
S.Po.C.sup.	superior postcentral sulcus
S.Rh.	rhinal sulcus
S.T.i.post.	posterior inferior temporal sulcus
S.T.s.	superior temporal sulcus
S.T.s.ter.asc.post.	posterior terminal ascending branch of the superior temporal sulcus
S.s.P.	sub-parietal sulcus
unknown	unknown cortical folds

Fig. 11. BrainVISA/Morphologist sulci atlas version 2011. The labels on each hemisphere are translated into English in the table below.

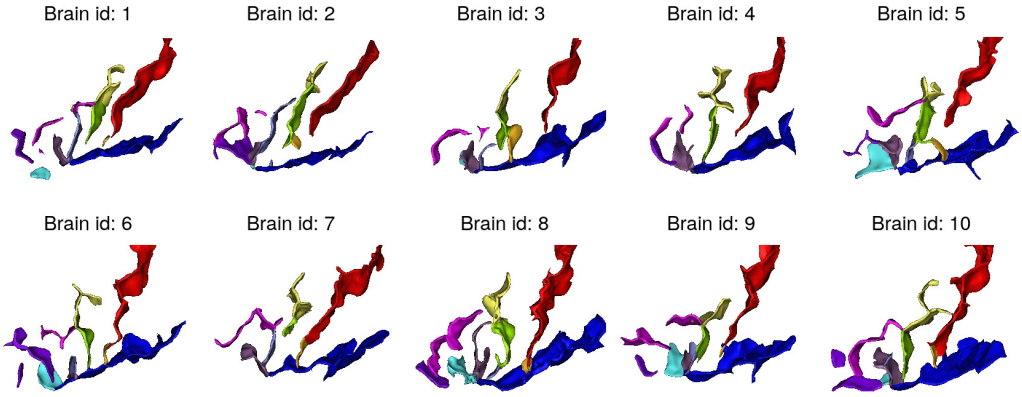

Fig. 12. Surrounding sulci of areas 44 and 45 of the first 10 Jülich brains.

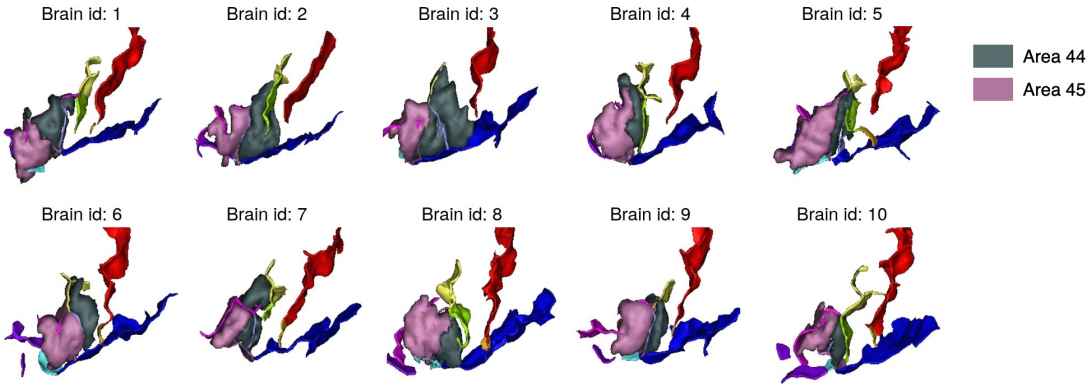

Fig. 13. Relationship between cytoarchitectonic areas 44, 45 and the corrected surrounding sulci for the left hemispheres of the first 10 Jülich brains. Sulcus colors have been updated to fit with the opinion of the anatomists, who did perform architectonic mapping and observed the folding configuration in the histological sections.